LEARNING NON-EQUILIBRIUM SIGNALING DYNAMICS IN SINGLE-CELL PERTURBATION DYNAMICS

Anonymous authors
Paper under double-blind review

ABSTRACT

Cancer cells exploit non-equilibrium signaling dynamics to develop transient drug resistance through mechanisms that conventional equilibrium-based analyses cannot detect. We present a probabilistic framework integrating live-cell biosensor data with asynchronous multi-omics snapshots to learn these adaptive states. Using data from $BRAF^{V600E}$ melanoma as a model system, we demonstrate how such learning scheme characterize competing timescales drive resistance mechanisms: rapid post-translational feedback (minutes) versus delayed transcriptional regulation (hours), including RAF dimer rewiring, DUSP-mediated ERK reactivation pulses, and $NRAS^{Q61K}$-dependent EGFR recycling. Our approach further combines multi-marginal Schrödinger bridges for distribution alignment with the extracted dynamical patterns from live-cell trajectories. Each step of the algorithm is validated with real-data and further validation is through in silico melanoma models. This framework could help identify therapeutic windows that delay progression to persistent resistant states and targeting adaptive plasticity across cancer types.

1 INTRODUCTION

Modern biology has witnessed a revolution in single-cell technologies, enabling unprecedented resolution in profiling cellular states. Techniques such as multiplexed iterative immunofluorescence imaging (Lin et al., 2018) and live-cell biosensors (Cutrale et al., 2017) now allow researchers to map protein expression, post-translational modifications, and signaling activity across millions of individual cells under diverse perturbations. These advances are particularly valuable for drug discovery, where understanding heterogeneous responses to pathway inhibition targeted therapies is critical to overcoming resistance (Samatar & Poulikakos, 2014).

Cancer cells exhibit remarkable plasticity, maintaining a multi-attractor landscape even in homeostasis. In melanoma, spontaneous transitions between proliferative, invasive, and drug-tolerant states occur without external perturbation Roesch et al. (2010). When treated with drugs, cells are forced from these steady states into non-equilibrium transients. Within 24 hours of RAF/MEK inhibition, $BRAF^{V600E}$ melanoma cells shift from monomeric BRAF-driven ERK activation to RAS-mediated dimeric CRAF signaling (Fröhlich et al., 2023).

The adapted cells demonstrate complex signaling dynamics across multiple timescales. ERK activity pulses occur with 45-90 minute periodicity, driven by post-translational modifications occurring within seconds to minutes, EGFR receptor trafficking and recycling taking 10-30 minutes, and transcriptional feedback via DUSP/SPRY downregulation occurring over hours Fröhlich et al. (2023). Traditional analysis pipelines struggle with these dynamics due to combinatorial complexity—even 20 signaling proteins can generate over 10^5 biochemical species through modifications and complex formation Jamison (1975). Rule-based modeling approaches Faeder et al. (2005) show how allosteric drug effects propagate through this network via ΔG energy landscapes, while the Gibbs free energy difference governing drug-target interactions becomes time-dependent under rapid signaling transients Lavoisier (1789).

Current dimensionality reduction techniques compound these challenges by obscuring critical high-dimensional features and averaging out transient states that drive phenotypic outcomes. Our framework addresses this through optimal transport regularized by live-cell biosensors (**?**), preserving

both high-dimensional structure and temporal dynamics. More specifically, we propose a probabilistic framework that bridges asynchronous snapshot data with continuous live-cell trajectories. Rather than relying on deterministic flow maps, we model cellular responses as stochastic processes informed by partial observations. Our approach combines stochastic flow matching to align high-dimensional marginal distributions via unbalanced Schrödinger bridges (**?**) with spectral analysis of transient dynamics using delay embeddings (Takens, 198) and Koopman operator theory Giannakis (2019). Using melanoma as a testbed, we demonstrate how these methods reveal coherent dynamics in drug resistance and predict context-dependent phenotypic outcomes, offering a framework for combining high-throughput and live-cell modalities.

Challenges in Cell Perturbation Analysis Transforming the data from high-throughput single-cell perturbation experiments into predictive dynamical models presents three fundamental challenges. First, temporal discontinuity arises from destructive measurement techniques that yield asynchronous marginal distributions $q(x_0), q(x_1), \ldots, q(x_T)$ at discrete timepoints, destroying cells during measurement. While the slow, quasi-equilibrium case can be addressed using multi-marginal optimal transport, drug perturbations often trigger rapid transitions occurring faster than typical sampling intervals, making displacement interpolation of the measures unreliable. The second challenge stems from limitations in traditional dimensionality reduction techniques like UMAP. These methods cannot capture temporal evolution in their static embeddings and often fragment transient states into disconnected clusters. The third challenge involves non-equilibrium dynamics: Drug perturbations drive cells into turbulent-like regimes where small initial differences amplify exponentially. This exponential amplification makes local distances unreliable predictors of cell fate and significantly complicates trajectory reconstruction from snapshots. The chaotic nature of these systems fundamentally limits our ability to make deterministic predictions about cellular responses to perturbations.

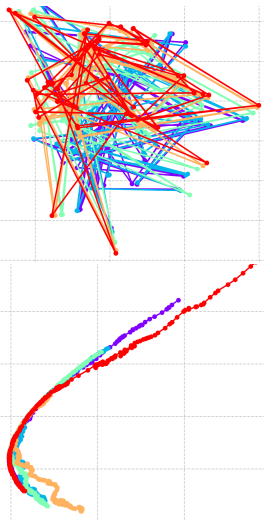

Figure 1: *UMAP embedding of 5 simulated cell trajectories with different colors in (top) snapshot data and (bottom) in live cell. Individual cell trajectories are shown in both cases despite their unavailability in snapshot data.*

Therefore, despite their effectiveness for unsupervised static methods, low-dimensional embeddings of single-cell snapshot data fall short for dynamical analysis (Kiselev et al., 2019; La Manno et al., 2018). Moreover, snapshot data captures many molecular species at intervals without cell tracking, while live cell data continuously monitors specific activities such as activation of key signaling molecules. Using snapshot data, UMAP (Figure 1, top) reveals a lower-dimensional manifold that lacks directional flow. In contrast, delay coordinate embedding of live cell data Takens (198); Packard et al. (1980) reveals structured trajectories (Figure 1, bottom).

Perturbations as Attractor-Kicking Events Cellular homeostasis evolves on a metastable manifold $\mathcal{M}_h \subset \mathbb{R}^d$ maintained by self-correcting biochemical networks (Fig. 2). It is common to assume this manifold acts as an attractor with dynamics governed by a potential field (Pillai & Jolly, 2021). The system's evolution can be formulated using the Fokker-Planck equation where the drug perturbations modify the drift term, creating transitions to alternative attractors $\mathcal{M}_i$:

$$X_t \xrightarrow{\text{Perturbation}} \begin{cases} \mathcal{M}'_h & \text{with rate } \lambda_1(X_{t^-}), \\ \mathcal{M}_{\text{res}} & \text{with rate } \lambda_2(X_{t^-}), \\ \mathcal{M}_{\text{death}} & \text{with rate } \lambda_3(X_{t^-}), \end{cases} \tag{1}$$

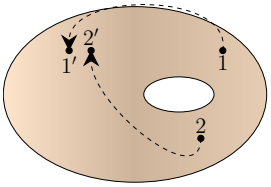

Figure 2: *A schematic of two dynamically adjacent cells that following non-homeostasis transients, settle back to homeostasis.*

where X_{t^-} is the pre-perturbation state. Here we focus on resistance mechanisms emerging on faster timescales, setting aside apoptosis and genetic/epigenetic alterations. Two cells are *dynamically adjacent* if their perturbed trajectories converge to the same attractor despite initial separation (see Fig. 2):

$$\lim_{t\to\infty} |X_i(t) - X_j(t)|_{\mathcal{M}_k} < \epsilon \implies i \sim j \tag{2}$$

2 REGULARIZED MULTI-MARGINAL FLOW MATCHING

To address these challenges, we propose a framework that combines high-dimensional snapshot data with live-cell biosensor measurements. Rather than relying on dimensionality reduction, which discards critical dynamical features, or integrating differential equations, which become intractable in high dimensions, we develop a robust simulation-free approach using spline measures, score matching, and live cell trajectory guidance. This integration is crucial: snapshot data provides comprehensive molecular states but lacks temporal resolution, while biosensor live data offers precise temporal information for selected molecules. We validate each step using experimental data and apply this framework to a mechanistic model of MAPK signaling, where we systematically evaluate biosensor selection based on information density, time-scale coverage, and pathway specificity. This approach represents a significant step toward understanding and potentially controlling cellular response to therapeutic perturbations.

2.1 ROBUST MULTI-MARGINAL FLOW MATCHING

Our framework addresses high-dimensional temporal modeling through three synergistic components that prevent overfitting while maintaining dynamical fidelity:

Spline-Decomposed Mini-Flows To handle irregular timepoints $\{t_i\}_{i=0}^{M}$, we construct the global flow as overlapping windows of spline measure triplets for observed marginals:

$$\mu_t = \sum_{i=0}^{M-k} B_i(t) \left[\mu_i + (t - t_i)\mathbf{v}_i\right], \quad t \in [t_i, t_{i+k}] \tag{3}$$

where $B_i(t)$ are B-spline basis functions with local support, $\mu_i = \mathbb{E}[\rho_i]$, and $\mathbf{v}_i$ are window-specific velocity fields. The B-spline construction ensures several important properties: It maintains C^2 smoothness between windows through basis function overlap, providing continuous transitions. Through localized parameter sharing, it has $\mathcal{O}(1)$ extra memory complexity to the previous scalable algorithms (Tong et al., 2023), making it computationally efficient.

Score-Matched Stochastic Dynamics Similar to Tong et al. (2023), we regularize the deterministic flow with learned stochastic components via score matching:

$$\mathcal{L}_{\text{score}} = \mathbb{E}_{t,x\sim p_t}\left[|s_\theta(x,t) - \nabla_x \log p_t(x)|^2\right] \tag{4}$$

where corrupted samples $\tilde{x} = x + \sigma(t)\epsilon$ use a Brownian bridge noise schedule $\sigma(t) = \sqrt{t(1-t)}$. This approach avoids explicit density estimation in high dimensions, captures uncertainty through stochastic differential equations, and prevents mode collapse via noise-adaptive regularization.

Live-Cell Biosensor Anchoring Experimental trajectories $y_j(t)$ from biosensors constrain the learned velocity field through a direct matching term:

$$\mathcal{L}_{\text{live}} = \sum_j \int_{t_{\text{min}}}^{t_{\text{max}}} |\mathbf{v}(y_j(t),t) - \dot{y}_j(t)|^2 dt \tag{5}$$

This coupling to continous dynamics serves multiple purposes. It enables physics-informed learning by directly matching observed velocities, provides multi-scale alignment by bridging biosensor measurements at $\mu m/\text{min}$ resolution with snapshot hour-scale data, and offers pathway specificity where channel selection (such as pERK versus RAS) determines the dynamical focus of the model via a *subset-correspondence* regularity on the optimal transport (Liu et al., 2019).

Theoretical Guarantees The combined framework provides several key theoretical guarantees. The divergence matching between the velocity field and score function ($\nabla \cdot \mathbf{v} = \nabla \cdot s_\theta$) ensures consistency with the Fokker-Planck equation. The incorporation of live-cell data resolves the drift-diffusion ambiguity inherent in stochastic differential equations. Additionally, the local nature of spline measures ensures bounded Lipschitz constants across time windows, providing stability to the framework.

Real Data Validation Applied to CITEseq and Multiome gene expression datasets measuring 50-1000 molecular features at irregular intervals (2-7 days) (Burkhardt et al., 2022), our framework demonstrates robust performance across dimensionality reduction strategies. For the 1000-dimensional highly-variable genes (Hi-Var 1000), Triplet-MMSFM achieves near-identical W_1 distances (50.64 vs 50.71) to Pairwise while reducing W_2^2 significantly, indicating precise distribution matching in higher dimensions. The model maintains stability across preprocessing methods, while maximum mean miscrepancy metrics reveal consistent pattern capture. This performance persistence across 50-1000 features and 4-7 day intervals confirms the method's capacity to handle biological noise and temporal sparsity inherent in real perturbation studies.

2.2 Operator-Theoretic Regularization for Flow Matching

Direct application of equation (5) may be unreliable because single cell trajectories contain both measurement noise and inherent chaotic dynamics. This makes velocity matching susceptible to overfitting temporary fluctuations rather than capturing true biological patterns. To address this, we employ Koopman operator theory (Mauroy et al., 2020) to decompose trajectories into coherent dynamical patterns that provide regularization constraints for the flow matching process. The Koopman operator $\mathcal{K}$ linearly advances observables $g(x)$ in time via $\mathcal{K}g(x_t) = g(x_{t+\Delta t})$, even when the underlying system exhibits nonlinear dynamics. Spectral decomposition of $\mathcal{K}$ yields eigenfunctions ϕ_j encoding predictable states and eigenvalues $\lambda_j = e^{(\theta_j + i\omega_j)\Delta t}$, where θ_j and ω_j govern growth/decay rates and oscillation frequencies, respectively.

For observed trajectories of molecular activity, $y(t)$, we approximate Koopman eigenfunctions from the eigenfunctions of Markov kernel operators constructed over delay-embedded states $Y(t) = [y(t), y(t-\tau), \ldots, y(t-(d-1)\tau)]$ (see Giannakis (2019)). This reveals dominant modes ϕ_1, ϕ_2 corresponding to drug response adaptation phases and oscillatory feedback. These data-driven modes replace the flow matching penalty (5) with the spectral signatures of the live cell dynamics. This loss enforces preservation of coherent temporal patterns. The regularization anchors the flow to biologically interpretable dynamics: eigenfunction gradients $\nabla\phi_j$ localize to key signaling nodes like DUSP6 and SPRY2, validating their roles as dynamical bottlenecks. By bridging data-driven pattern extraction with mechanistic interpretability, this operator-theoretic approach ensures robust generalization despite trajectory-level unpredictability.

2.2.1 Experimental Validation

Application to BRAF^{V600E} melanoma cells under ERK inhibition revealed three key findings. First, delay-embedded ERK trajectories exhibited block-diagonal kernel structure, indicating predictable states, and two dominant Koopman modes (Fig. 3). The first mode exhibited slow decay capturing ERK suppression, while the second mode shows oscillations from negative feedback.

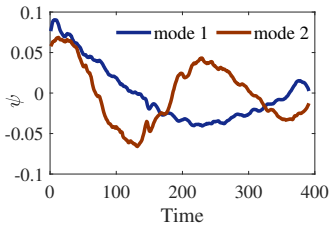

Figure 3: The first two extracted principal Koopman modes.

Figure 4 demonstrates our framework's ability to reconstruct ERK trajectories in the Low ERKi training condition (left) and generalize to unseen High ERKi data (right). Compared to Probabilistic Linear Dynamical Systems (PLDS) Chen et al. (2017)–a conventional approach modeling dynamics through low-dimensional linear transitions with Gaussian noise–our operator-based method maintains phase coherence in unseen conditions where PLDS trajectories diverge rapidly

Remark: Biological systems under perturbation exhibit inherent non-ergodicity in time, yet modern single-cell technologies provide spatial ergodicity through simultaneous measurements of millions of cells. This allows approximation of temporal averages by ensemble averages: $\mathbb{E}_t[f(X_t)] \approx \mathbb{E}_{x\sim q_t}[f(x)]$, where q_t is the empirical distribution at time t. Here, rather than attempting to construct exact flow maps, we focus on extracting predictable patterns using the transition density function $p_\tau : \mathbb{X} \times \mathbb{X} \to [0, \infty)$, which quantifies $\mathbb{P}[\Phi_\tau(\mathbf{X}_t) \in \mathbb{A} | \mathbf{X}_t = x]$ for any measurable subset $\mathbb{A} \subset \mathbb{X}$.

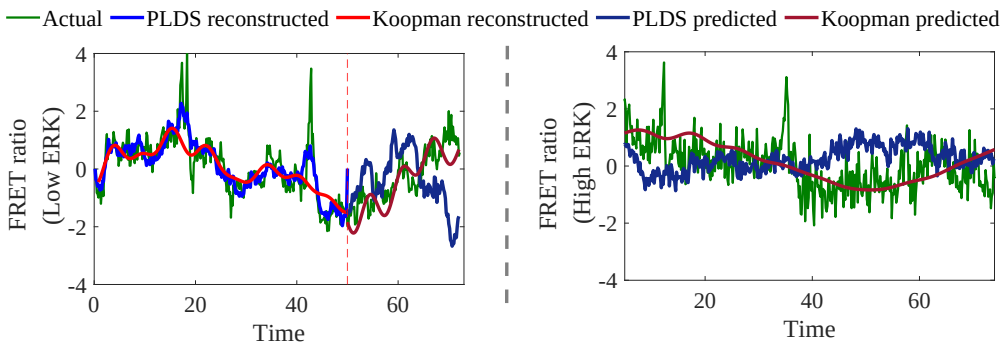

Figure 4: *Performance examples of model prediction for ERK activity trajectories in the Low ERKi condition (left, training set) and High ERKi condition (right, test set).*

3 In-Silico Validation with Mechanistic models

While operator-theoretic regularization demonstrates promising results in biological data, rigorous validation of the learning algorithm necessitates controlled environments with fully known dynamics. We address this through a high-fidelity in-silico MAPK/AP-1 network model that replicates $\text{BRAF}^{\text{V600E}}$ melanoma signaling at single-molecule resolution developed by Fröhlich et al. (2023). This computational model of $\text{BRAF}^{\text{V600E}}$ melanoma captures allosteric regulation, transcriptional feedback, and compartmentalization through 68 mechanistic rules that generate over 100,000 reactions.

The model provides two parameterizations: a base model for generic RAF/MEK inhibition studies, and a specialized pRAF model calibrated for p-RAF inhibitors with adjusted $\Delta\Delta G$ values for RAF dimer allostery, specific phosphorylation rules for CRAF(S642) and BRAF(T753), and modified MEK-ERK binding kinetics. The rule-based architecture is built on fundamental biochemical processes. Binding interactions, comprising 23 rules, include key processes such as BRAF-MEK binding: $\text{BRAF} + \text{MEK}^u \underset{k_{-1}}{\overset{k_1}{\rightleftharpoons}} \text{BRAF:MEK}^u$. Catalytic reactions, described by 24 rules, follow Michaelis-Menten kinetics, as exemplified by MEK phosphorylation of ERK: $v = \frac{k_{\text{cat}}[\text{MEK}^p][\text{ERK}]}{K_m + [\text{ERK}]}$.

Thermodynamic constraints are encoded through energy patterns, particularly for RAF dimer stabilization by inhibitors: $\Delta\Delta G_{\text{bind}} = -RT \ln\left(\frac{[\text{RAFi:RAF}_2]}{[\text{RAFi}][\text{RAF}]^2}\right) + \Delta\Delta G_{\text{allostery}}$ for pan-RAF inhibitors. The model classifies biochemical interactions into six fundamental types: GTP exchange, gene expression, phosphorylation, endosomal shuttling, dephosphorylation, and drug inhibition. Each type is represented by specific mathematical formulations and experimentally derived parameters. For example, gene expression follows $\frac{d[\text{DUSP}]}{dt} = \alpha_{\text{DUSP}}[\text{pERK}] - \delta_{\text{DUSP}}[\text{DUSP}]$, while drug inhibition is governed by binding energies $\Delta G_{\text{bind}} = -RT \ln\left(\frac{[\text{RAFi-RAF}]}{[\text{RAFi}][\text{RAF}]}\right)$.

The model has been extensively validated, achieving RMSD ¡15% for ERK activity trajectories and Pearson $R = 0.91$ for drug synergy predictions. These results demonstrate key biological insights: RAF inhibitor efficacy depends strongly on dimerization energetics, MEK inhibitor resistance emerges through DUSP6 feedback mechanisms, and $\text{NRAS}^{\text{Q61K}}$ mutation substantially reduces the EC_{50} for EGF by 83%.

3.1 Optimal Biosensor Selection for MAPK Signaling Dynamics

The MAPK pathway exhibits complex dynamics involving allostery, feedback, and adaptive rewiring Fröhlich et al. (2023). We propose a sensor set to maximize information capture from live-cell imaging, enabling accurate alignment and reconstruction of high-dimensional snapshot data. Assume four key molecules: pERK (phosphorylated ERK), which integrates signals from

BRAF(V600E) and RAS-driven pathways with pulsatile dynamics measured via FRET-based biosensor; RAS-GTP (active RAS), which initiates RAF dimerization and MAPK activation measured using GFP-tagged RAS-binding domain probe; pMEK (phosphorylated MEK), which acts as a convergence node for BRAF(V600E) monomers and RAS-driven RAF dimers measured via antibody-based live-cell biosensor; and DUSP mRNA, which provides slow transcriptional feedback measured via MS2 stem-loop system.

These sensors were selected to maximize information through coverage of BRAF(V600E) and RAS channels, time-scale heterogeneity from seconds to hours, and mutual information minimization for redundancy reduction: i.e. $I(\text{pERK}; \text{DUSP mRNA} | \text{pMEK})$. The temporal alignment strategy leverages the heterogeneous time scales of these sensors, with RAS-GTP capturing pulse initiation (seconds), pMEK/pERK tracking signal propagation (minutes), and DUSP mRNA reflecting transcriptional memory (hours). Flow matching is implemented with the added regularity to the loss function (Equation (5)).

4 Discussion

Our framework fundamentally reorients single-cell perturbation analysis from alignments of static snapshots to dynamic process reconstruction. By combining multi-marginal Schrödinger bridges with spectral operators, we attack a critical paradox in systems biology: how to preserve high-dimensional molecular states while capturing transient dynamics essential for predicting cellular decision-making. This approach reveals several key mechanistic insights into drug resistance and how early molecular events orchestrate subsequent cell fate decisions.

Our operator-theoretic approach provides spectral regularization that preserves coherent and predictable transient valleys in the dynamic landscape where the traditional dimensionality reduction methods collapse. Delay-embedded Koopman modes successfully reconstruct unmeasured JUN/ATF dynamics from ERK biosensors alone, while causal optimal transport disentangles minute-scale phosphorylation from hour-scale transcription. Notably, preliminary in silico validation achieved early resistance prediction, demonstrating the framework's practical utility. In other words, though highly variable at the single-cell level, contain predictive patterns when viewed through the lens of operator theory. The Koopman decomposition of live-cell trajectories identifies coherent modes of behavior that emerge during the initial response to perturbation.

Looking forward, several challenges remain. The careful selection of biosensors proves essential for capturing the multi-scale nature of cellular response. Our chosen set spans timescales from seconds to hours, providing temporal anchors that constrain the flow matching problem. This temporal hierarchy enables robust reconstruction of transition paths that would be invisible to the null alignment of optimal transport alone. Integrating mitotic history as covariates of the dynamic bridges could resolve heritable versus stochastic resistance mechanisms. Realizing the full potential of this approach demands developing benchmark datasets with time-matched live/snapshot pairs, and establishing mechanistic taxonomies for drug responses based on dynamical signatures. Consequently, our framework represents a significant advance in resolving early transient responses to perturbation. It demonstrates that the era of equilibrium-focused single-cell biology must yield to a dynamical paradigm that embraces turbulence as fundamental, not artifact. As biological reality flows, our models must learn to navigate its currents rather than seek frozen snapshots of its waves.

References

Daniel B Burkhardt, Beatriz P San Juan, John G Lock, Smita Krishnaswamy, and Christine L Chaffer. Mapping phenotypic plasticity upon the cancer cell state landscape using manifold learning. *Cancer Discovery*, 12(8):1847–1859, 2022.

Shaojie Chen, Kai Liu, Yuguang Yang, Yuting Xu, Seonjoo Lee, Martin Lindquist, Brian S Caffo, and Joshua T Vogelstein. An m-estimator for reduced-rank system identification. *Pattern recognition letters*, 86:76–81, 2017.

Francesco Cutrale, Vikas Trivedi, Le A Trinh, Chi-Li Chiu, John M Choi, Marcela S Artiga, and Scott E Fraser. Hyperspectral phasor analysis enables multiplexed 5d in vivo imaging. *Nature methods*, 14(2):149–152, 2017.

James R Faeder, Michael L Blinov, Byron Goldstein, and William S Hlavacek. Rule-based modeling of biochemical networks. *Complexity*, 10(4):22–41, 2005.

Fabian Fröhlich, Luca Gerosa, Jeremy Muhlich, and Peter K Sorger. Mechanistic model of mapk signaling reveals how allostery and rewiring contribute to drug resistance. *Molecular Systems Biology*, 19(2):e10988, 2023.

Dimitrios Giannakis. Data-driven spectral decomposition and forecasting of ergodic dynamical systems. *Applied and Computational Harmonic Analysis*, 47(2):338–396, 2019.

Benton Jamison. The Markov processes of schrödinger. *Zeitschrift für Wahrscheinlichkeitstheorie und verwandte Gebiete*, 32(4):323–331, 1975.

Vladimir Yu Kiselev, Tallulah S Andrews, and Martin Hemberg. Challenges in unsupervised clustering of single-cell rna-seq data. *Nature Reviews Genetics*, 20(5):273–282, 2019.

Gioele La Manno, Ruslan Soldatov, Amit Zeisel, Emelie Braun, Hannah Hochgerner, Viktor Petukhov, Katja Lidschreiber, Maria E Kastriti, Peter L"onnerberg, Alessandro Furlan, and J Fan. Rna velocity of single cells. *Nature*, 560(7719):494–498, 2018.

Antoine Lavoisier. Traité élémentaire de chimie, présenté dans un ordre nouveau et d'apres les découvertes modernes, 2 vols. *Cuchet libraire, Paris*, 1789.

Jia-Ren Lin, Benjamin Izar, Shu Wang, Clarence Yapp, Shaolin Mei, Parin M Shah, Sandro Santagata, and Peter K Sorger. Highly multiplexed immunofluorescence imaging of human tissues and tumors using t-cycif and conventional optical microscopes. *Elife*, 7, 2018.

Ruishan Liu, Akshay Balsubramani, and James Zou. Learning transport cost from subset correspondence. *arXiv preprint arXiv:1909.13203*, 2019.

Alexandre Mauroy, Igor Mezic, and Yoshihiko Susuki. *The Koopman Operator in Systems and Control: Concepts, Methodologies, and Applications*. Springer, 2020. doi: 10.1007/978-3-030-35713-9.

Norman H Packard, James P Crutchfield, J Doyne Farmer, and Robert S Shaw. Geometry from a time series. *Physical review letters*, 45(9):712, 1980.

Maalavika Pillai and Mohit Kumar Jolly. Systems-level network modeling deciphers the master regulators of phenotypic plasticity and heterogeneity in melanoma. *IScience*, 24(10), 2021.

Alexander Roesch, Adina Vultur, Ivan Bogeski, Huan Wang, Katharina M Zimmermann, David Speicher, et al. Overcoming intrinsic multidrug resistance in melanoma by blocking the mitochondrial respiratory chain of slow-cycling jarid1b high cells. *Cancer Cell*, 18(2):145–157, 2010.

Ahmed A Samatar and Poulikos I Poulikakos. Targeting ras–erk signalling in cancer: promises and challenges. *Nature reviews Drug discovery*, 13(12):928–942, 2014.

Floris Takens. Detecting strange attractors in turbulence. In *Dynamical Systems and Turbulence, Warwick 1980: proceedings of a symposium held at the University of Warwick 1979/80*, pp. 366–381. Springer, 198.

Alexander Tong, Nikolay Malkin, Kilian Fatras, Lazar Atanackovic, Yanlei Zhang, Guillaume Huguet, Guy Wolf, and Yoshua Bengio. Simulation-free schr\" odinger bridges via score and flow matching. *arXiv preprint arXiv:2307.03672*, 2023.